# The NO*v*A simulation chain



2015 J. Phys.: Conf. Ser. 664 072002

(http://iopscience.iop.org/1742-6596/664/7/072002)

Journal of Physics: Conference Series **664** (2015) 072002 doi:10.1088/1742-6596/664/7/072002

# The NO$\nu$A simulation chain

**A Aurisano[1], C Backhouse[2], R Hatcher[3], N Mayer[4], J Musser[5], R Patterson[2], R Schroeter[6], and A Sousa[1]**

[1]University of Cincinnati, Cincinnati OH, USA
[2]California Institute of Technology, Pasadena CA, USA
[3]Fermi National Accelerator Laboratory, Batavia IL, USA
[4]Tufts University, Medford MA, USA
[5]Indiana University, Bloomington IN, USA
[6]Harvard University, Cambridge, MA, USA

E-mail: aurisaam@ucmail.uc.edu, bckhouse@caltech.edu, rhatcher@fnal.gov, nathan.mayer@tufts.edu, jmusser@indiana.edu, rbpatter@caltech.edu, rschroet@physics.harvard.edu, Alex.Sousa@uc.edu

**Abstract.** The NO$\nu$A experiment is a two-detector, long-baseline neutrino experiment operating in the recently upgraded NuMI muon neutrino beam. Simulating neutrino interactions and backgrounds requires many steps including: the simulation of the neutrino beam flux using FLUKA and the FLUGG interface; cosmic ray generation using CRY; neutrino interaction modeling using GENIE; and a simulation of the energy deposited in the detector using GEANT4. To shorten generation time, the modeling of detector-specific aspects, such as photon transport, detector and electronics noise, and readout electronics, employs custom, parameterized simulation applications. We will describe the NO$\nu$A simulation chain, and present details on the techniques used in modeling photon transport near the ends of cells, and in developing a novel data-driven noise simulation. Due to the high intensity of the NuMI beam, the Near Detector samples a high rate of muons originating in the surrounding rock. In addition, due to its location on the surface at Ash River, MN, the Far Detector collects a large rate ( $\sim$140 kHz) of cosmic muons. We will discuss the methods used in NO$\nu$A for overlaying rock muons and cosmic ray muons with simulated neutrino interactions and show how realistically the final simulation reproduces the preliminary NO$\nu$A data.

## 1. Introduction

NO$\nu$A [1] is a two-detector, long-baseline neutrino oscillation experiment located 14 mrad off-axis from the NuMI neutrino beam and is designed to measure the oscillation probabilities for $\nu_\mu \to \nu_e$ and $\bar{\nu}_\mu \to \bar{\nu}_e$. The probabilities will allow us to study the mass ordering of the three neutrino species as well as constrain the charge-parity violating phase in the leptonic sector. NO$\nu$A can also measure the oscillation probabilities for $\nu_\mu \to \nu_\mu$ and $\bar{\nu}_\mu \to \bar{\nu}_\mu$ to improve the precision with which we know $|\Delta m^2_{32}|$ and $\theta_{23}$.

The NuMI beam, originally built to supply neutrinos to the MINOS experiment, is produced by the NuMI facility [2] shown in Fig. 1. The beam begins with 120 GeV protons from the Main Injector striking a graphite target. The resulting particles are focused by two magnetic focusing horns. Particles then travel down the decay pipe to allow pions to decay to muons and neutrinos. Muons and any remaining hadrons are absorbed in rock leaving a beam of only neutrinos. The focusing horns can run in two modes: in forward horn current mode, the horns

focus $\pi^+$ and defocus $\pi^-$ resulting in a nearly pure $\nu_\mu$ beam; reversing the horn current focuses $\pi^-$ resulting in a $\bar{\nu}_\mu$ enriched beam. After upgrades in preparation for the NO$\nu$A experiment, the NuMI beam now runs in medium energy mode with a peak energy of ~8 GeV.

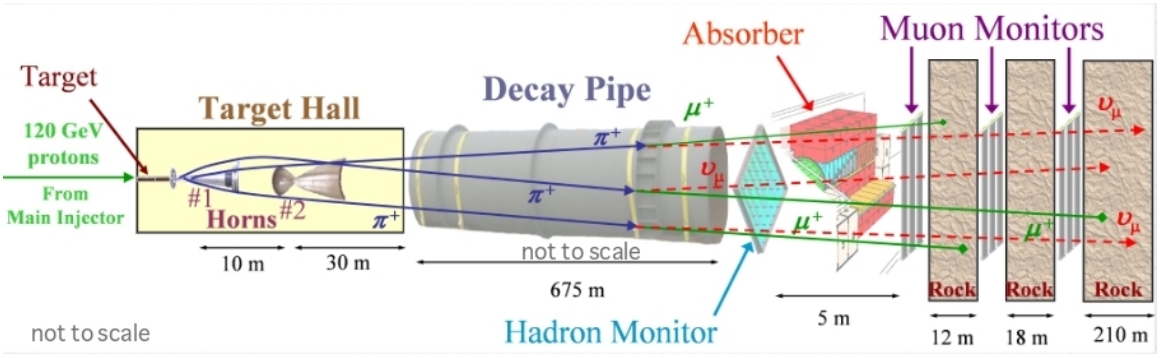


**Figure 1.** A schematic of the NuMI facility. The NuMI beam can run in a $\nu_\mu$ mode or a $\bar{\nu}_\mu$-enriched mode by changing the direction of the current in the magnetic focusing horns.

The NO$\nu$A detectors are low Z tracking calorimeters composed of alternating vertical and horizontal planes of liquid scintillator filled PVC cells. Light is transported out of the cells using wave-length shifting fiber loops that are read out by avalanche photodiodes (APDs). Far detector cells are 15.6 m long while near detector cells are 4.2 m long. Cells in both the near and far detectors have a 4 cm × 6 cm cross-section. The far detector (Fig. 2) is 15.6 m × 15.6 m × 60 m with a mass of 14 kton and ~344,000 cells. The near detector (Fig. 3) is 4.2 m × 4.2 m × 15.8 m with a mass of 0.3 kton and ~20,000 cells. The near detector is designed to be functionally equivalent to the far detector to allow for systematic uncertainty cancellation. To handle the high rate environment of the near detector cavern, the near detector is outfitted with 4x faster electronics than the far detector. As seen in Fig. 4 the far detector is located near Ash River, Minnesota, 810 km from the NuMI target. The near detector is located on the Fermilab campus 1 km from the NuMI target. Both detectors are 14 mrad off-axis to create a 2 GeV narrow-band beam.

**Figure 2.** The NO$\nu$A far detector seen from the top.

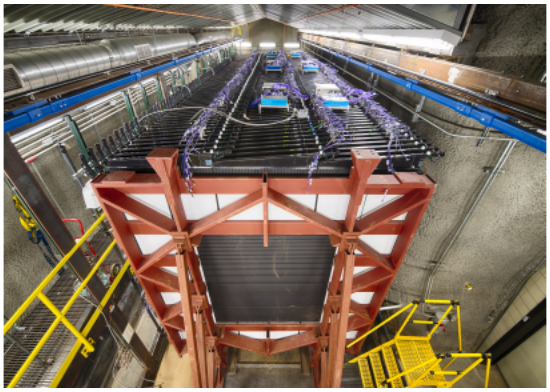

**Figure 3.** The NO$\nu$A near detector seen from the front.

The steps to simulate neutrino interactions and backgrounds are illustrated in Fig. 5. The simulation of neutrino interactions starts with modeling hadron production within the target,


**Figure 4.** The locations of the near and far detector, and the path of the NuMI beam. The detector are located off the path of the beam (off-axis) to select neutrinos with energies narrowly distributed around 2 GeV.

focusing in the horns, and downstream tertiary production to determine the production rate and energy spectrum of each neutrino flavor from the decay of pions, kaons, and muons in the decay pipe using the FLUKA simulation package [3, 4] and the FLUGG GEANT4 geometry interface [5]. The resulting simulated neutrinos are stored in flux files along with information about their parentage, and they are used as inputs to the neutrino event generation stage performed with GENIE [6]. Factorizing out the simulation of the neutrino flux from the rest of the simulation minimizes the number of times this computationally intensive step needs to be run as well as allowing for after the fact tunings of hadron production or focusing parameters. Since the far detector is on the surface, cosmic rays are a significant background; we generate cosmic ray events with CRY [7]. The particle lists generated by either GENIE or CRY are then passed to GEANT4 [8, 9], which propagates particles through the detector and produces energy deposits in active material. Finally, the list of energy deposits in active material are passed to a parameterized front-end simulation which converts energy deposits into scintillation light, transports scintillation light to the APD, and simulates the readout electronics response. The final output is formatted like raw data.

Due to the high beam intensity at the near detector, many neutrinos interact in the rock in front of the detector. Simulating these interactions requires allowing GEANT4 to propagate muons through a very large rock volume which is a slow process, and only a few of these muons will make it into our detector. To correctly account for this, we simulate many neutrino interactions with the mother volume including a large rock volume in front of the detector, and only keep those that leave energy in the detector. During normal simulation, with the mother volume only including the detector and the immediate detector hall, we overlay these rock 'singles' at a rate determined during the generation of flux files after the GEANT4 stage.

## 2. Photon Transport

While GEANT4 is capable of simulating optical photon processes, generating scintillation light and propagating it through the cell, up the fiber, and to the APD is very time consuming. Instead, we observe that the NO$\nu$A detectors are composed of many identical readout cells as shown in Fig. 6, so if we can generate templates to parameterize photon transport once, we can use them everywhere. The processes we must be able to parameterize are: the collection of scintillation photons by the fiber, the transport of light up the fiber, and the response of the

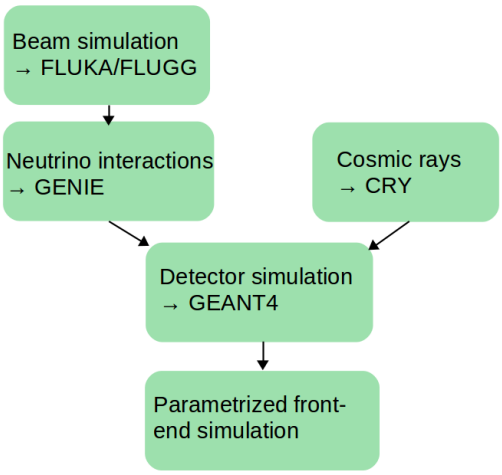


**Figure 5.** Steps in the simulation chain for the NO$\nu$A experiment

APD to the captured light.

To understand the collection of scintillation photons by the fiber, we developed a ray tracing simulation which uses the measured scintillation spectrum of the liquid scintillator, the average measured reflectivity of the PVC cell walls, and the absorption spectrum of the wavelength shifting fibers. Fig. 7 shows the resulting collection rate as a function of the distance along the length of the cell between where the photon was collected relative to the its origin ($\Delta Z$) and the time when the photon was collected relative to its emission ($\Delta T$).

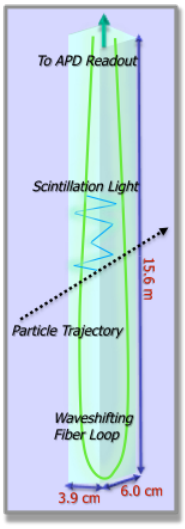


**Figure 6.** A schematic of the readout cell, the basic building block of the NO$\nu$A detectors.

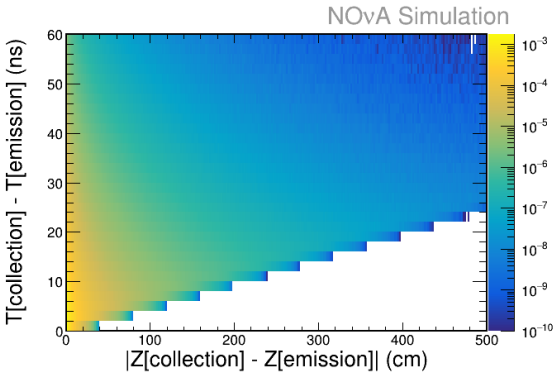


**Figure 7.** The collection rate of scintillation photons by a wavelength shifting fiber loop as estimated by a custom ray tracing simulation.

In the final simulation, this distribution is shifted to the position along the cell where GEANT4 has placed an energy deposit and is multiplied by the visible deposited energy and

a factor to convert energy to scintillation photons. The upper manifold and the lower end cap of the readout cell have low reflectivity. We approximate this by truncating any portion of the template laying outside of the cell. At this point, we have the mean number of photons captured as a function of $\Delta Z$.

Next, we must transport the photons up the fiber to determine the number of photons absorbed by the APD as a function of time. For a given bin in $\Delta Z$, we transport half of the collected photons up the long path around the fiber loop while the other half are transported up the short path. The mean number of photons surviving after being transported around the fiber is determined using an attenuation curve shown in Fig. 8 constructed from the average over the quality control tests of many spools of wavelength shifting fiber. After accounting for the quantum efficiency of the APD and Poisson sampling, we have the number of photoelectrons absorbed by the APD for a given $\Delta Z$ bin. The timing of photons is determined by the sum of the time of the GEANT4 energy deposit, the $\Delta T$ due to propagation in the scintillator drawn from the 1D projection of the photon collection template at a fixed $\Delta Z$, and the propagation time up the fiber. Since the apparent speed of photon propagation in the fiber depends on the angle of propagation (and hence the true path length), we draw from a template constructed from the travel time up the fiber divided by the travel distance as calculated by a fiber ray tracing simulation. Once photons from all $\Delta Z$ bins have been propagated to the APD, we have the number of photo-electrons as a function of time for a given energy deposit.

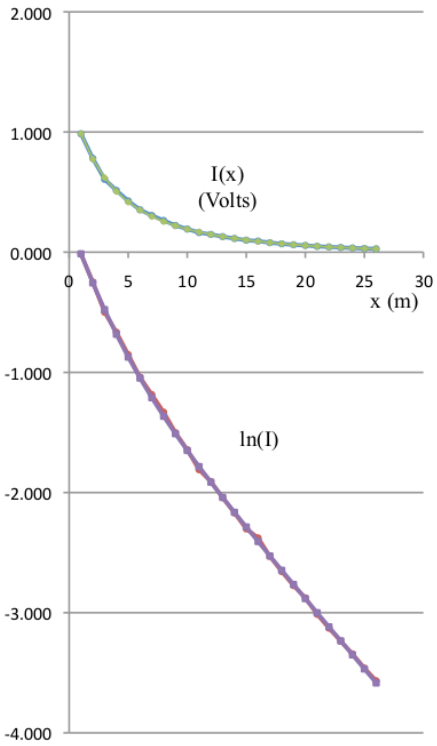


**Figure 8.** The attenuation curve, used to convert photons collected by the fiber to photons transported to the APD, shown in linear and log scales. As can be seen from the log scale version, the curve can be adequately approximated as a double exponential.

In addition to the Poisson variation induced by the number of photoelectrons ($N_{pe}$) captured by the APD, APDs have an excess noise factor (F) that expands the variance of the detected signal from $N_{pe}$ to $F*N_{pe}$. The theoretical distribution of the APD response is known [10], but it is difficult to randomly sample. Since the avalanche amplification process in an APD consists of many random charge multiplications, and the log-normal distribution can be considered the limit of the product of many independent random variables, we model the theoretical distribution as

$N_{pe}$ Poisson sampled with a mean value of $\bar{N}_{pe}$ and multiplied by a scale factor sampled from a log-normal distribution a mean of 1 and a variance of $(F-1)/N_{pe}$. This preserves the mean of the Poisson distribution while correctly expanding the variance to account for excess noise. As seen in Fig. 9, the log-normal expanded photoelectron distribution matches the theoretical distribution well.

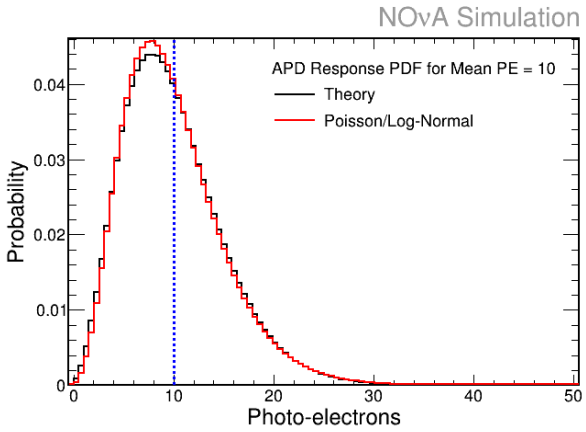


**Figure 9.** A comparison of APD response distribution from theory to simulation using a log-normal distribution.

## 3. Electronics Simulation

The goal of the electronics simulation is to convert the distribution of excess noise expanded photoelectrons as a function of time from the photon transport stage into digital signals similar to those collected from the detector. The front-end boards that this step emulates contain three chips: an ASIC which performs pulse shaping, and ADC which converts the shaped analog signals into digital signals, and an FPGA which performs real-time zero suppression.

The pulse shaping in the ASIC is performed by a CR-RC circuit. Therefore, we create analog traces in units of photoelectrons using the equation:

$$f(t) = N_{pe}\frac{F}{F-R}\left(e^{-(t-t_0)/F} - e^{-(t-t_0)/R}\right) \tag{1}$$

where $t_0$ is the time that the photoelectron pulse was collected by the APD, $F$ is the fall time of the CR-RC circuit, and $R$ is the rise time of the CR-RC circuit.

Next, we add electronics noise. In cells with energy deposits, we add a noise trace modeled by the sum of two Gaussian Markov chains representing current and voltage noise sources to the physics trace. The voltage noise component is of the form:

$$V_i = \frac{T_{read}}{R+T_{read}}Z_i + \frac{R}{R+T_{read}}V_{i-1} \tag{2}$$

where $T_{read}$ is the time between digitization (500 ns for the far detector and 125 ns for the near detector) and $Z_i$ is random number drawn from the unit Gaussian distribution. The current noise component is of the the form:

$$C_i = \frac{T_{read}}{F+T_{read}}Z_i + \frac{F}{F+T_{read}}C_{i-1} \tag{3}$$

and the final noise trace is $aV_i + bC_i$ where $a$ and $b$ are determined through a fit to pedestal scans. To save time for cells with no energy deposits, we distribute unclustered hits extracted from real data.

At this stage, we convert the trace from units of photoelectrons to ADC using a factor determined through charge injection studies. We add a baseline drawn from the distribution of modes seen in pedestal scan, and truncate to integers. Finally, we emulate the real-time zero suppression performed by the FPGA by looking for peaks above threshold in the dual correlated sampling trace defined as:

$$dcs_i = ADC_i - ADC_{i-3} \tag{4}$$

where $ADC_i$ is the value of the current digitization sample and $ADC_{i-3}$ is the value of the digitization sample three time slices earlier than the current one. In the real readout, thresholds are set on a channel-by-channel basis from periodic pedestal scans. In the simulation, we can draw thresholds from a distribution of thresholds seen at the real detector or use the actual thresholds recorded in the run conditions database.

## 4. Data/Monte Carlo Comparisons

Using the complete simulation, we can now compare low-level quantities in data and Monte Carlo. To keep our signal regions blind, we only look at cosmic ray data by ignoring any data taken during a beam spill trigger. The photoelectron spectrum for data and Monte Carlo can be seen in Fig. 10 for the near detector and Fig. 11 for the far detector. It is important to note that no offline calibrations have been applied, and the only tunings applied are the overall light level (photons per MeV) needed in the photon transport stage and the noise coefficients needed in the digitization stage. The peaks of the distributions agree well, and the effect of baseline variation on saturated hits can be seen at large photoelectron values.

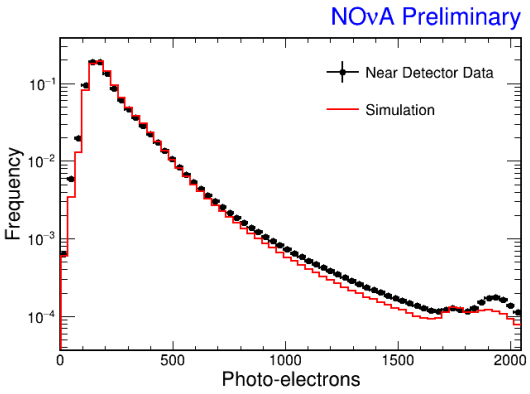


**Figure 10.** A comparison of the photoelectron spectrum in cosmic rays at the near detector in data and Monte Carlo.

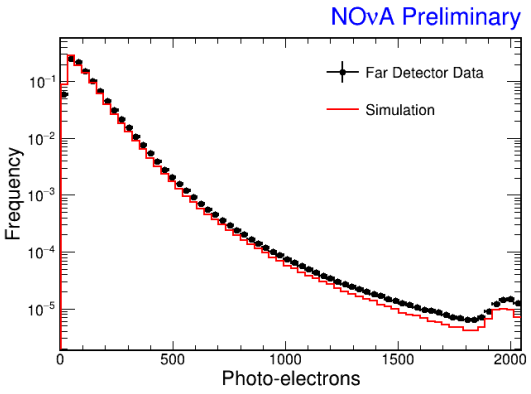


**Figure 11.** A comparison of the photoelectron spectrum in cosmic rays at the far detector in data and Monte Carlo.

## 5. Summary

Simulation at NO$\nu$A is a multi-stage process. For beam events this requires simulating the beam flux with FLUKA and the FLUGG GEANT geometry interface, generating neutrino interactions with GENIE, and simulating the energy deposited in active material with GEANT4. Cosmic rays, a major background at the far detector, are simulated using the CRY event generator.

The modeling of the collection and transport of scintillation light, the response of the APD, and the front-end boards is done by custom, parametrized modules. Preliminary results show that low-level quantities in cosmic ray data and Monte Carlo match well.

**Acknowledgements**
The author acknowledges support for this research was carried out by the Fermilab scientific and technical staff. Fermilab is operated by Fermi Research Alliance, LLC under contract No. De-AC02-07CH11359 with the United States Department of Energy.

**References**

[1] Ayres D *et al.* (NOvA Collaboration) 2007 The NOvA Technical Design Report Tech. Rep. FERMILAB-DESIGN-2007-01 Fermilab
[2] Anderson K *et al.* 1998 The NuMI Facility Technical Design Report Tech. Rep. FERMILAB-DESIGN-1998-01 Fermilab
[3] Bohlen T, Cerutti F, Chin M, Fasso A, Ferrari A, Ortega P, Mairani A, Sala P, Smirnov G and Vlachoudis V 2014 *Nucl. Data Sheets* **120** 211 – 214
[4] Ferrari A, Sala P R, Fasso A and Ranft J 2005 FLUKA: A multi-particle transport code (Program version 2005) Tech. Rep. CERN-2005-010 CERN
[5] Campanella M, Ferrari A, Sala P and Vanini S 1999 First Calorimeter Simulation with the FLUGG Prototype Tech. Rep. CERN-ATL-SOFT-99-004 CERN
[6] Andreopoulos C *et al.* 2010 *Nucl. Instrum. Meth.* A **614** 87–104
[7] Hagmann C, Lange D and Wright D 2007 *Nuclear Science Symp. Conf. Rec. (Honolulu, HI)* vol 2 (IEEE) pp 1143–1146
[8] Agostinelli S *et al.* 2003 *Nucl. Instrum. Meth.* A 250–303
[9] Allison J *et al.* 2006 *IEEE Trans. Nucl. Sci.* **53**(1) 270–278
[10] Balaban P, Fleischer P and Zucker H 1976 *IEEE Trans. Electron Devices* **23** 1189–1190